Published in final edited form as:
Nature. 2017 February 23; 542(7642): 498–502. doi:10.1038/nature21384.

Basis of catalytic assembly of the mitotic checkpoint complex

Alex C. Faesen[1,#], **Maria Thanasoula**[1], **Stefano Maffini**[1], **Claudia Breit**[1], **Franziska Müller**[1], **Suzan van Gerwen**[1], **Tanja Bange**[1], and **Andrea Musacchio**[1,2,#]

[1]Department of Mechanistic Cell Biology, Max-Planck Institute of Molecular Physiology, Otto-Hahn-Straße 11, 44227 Dortmund, Germany

[2]Centre for Medical Biotechnology, Faculty of Biology, University Duisburg-Essen, Universitätsstrasse, 45141 Essen, Germany

Abstract

Accurate genome inheritance by daughter cells requires that sister chromatids in the mother attach to microtubules emanating from opposite poles of the mitotic spindle (bi-orientation). A surveillance mechanism named the spindle assembly checkpoint (SAC) monitors the microtubule attachment process, temporarily halting sister chromatid separation and mitotic exit until completion of bi-orientation1. SAC failure results in abnormal chromosome numbers (aneuploidy), a hallmark of many tumours. The HORMA domain protein MAD2 is a subunit of the SAC effector mitotic checkpoint complex (MCC). Structural conversion from open to closed MAD2 is required for MAD2 incorporation in MCC1. *In vitro*, MAD2 conversion and MCC assembly requires several hours2–4, while the SAC response in cells is established in a few minutes5–7. To address this discrepancy, we reconstituted with purified components a near-complete SAC signalling system and monitored MCC assembly with real-time sensors. Dramatic acceleration of MAD2 conversion and MCC assembly was observed when MPS1 phosphorylated the MAD1:MAD2 complex, triggering its template function in the MAD2 conversion and contributing to the establishment of a physical platform for MCC assembly. Thus, catalytic activation of the SAC depends on regulated protein-protein interactions that accelerate the spontaneous but rate-limiting conversion of MAD2 required for MCC assembly.

Keywords

kinetochore; spindle checkpoint; cell division; mitosis; mitotic spindle; biochemical reconstitution; mitotic checkpoint complex; CDC20; BUBR1; BUB3; MAD2; MAD1; BUB1; MPS1

The SAC temporarily targets the activity of the E3 ubiquitin ligase anaphase promoting complex/cyclosome (APC/C), which is required for mitotic exit (Figure 1a). Two SAC

[#]Correspondence: alex.faesen@mpi-dortmund.mpg.de, andrea.musacchio@mpi-dortmund.mpg.de.

Author Contributions

A.C.F. and A.M. designed experiments and analysed results. A.C.F., M.T., C.B. and S.v.G. set up recombinant expression systems and purified proteins. A.C.F performed *in vitro* experiments. M.T. performed solid phase binding assays. S.M. and S.v.G. performed cellular SAC assays. F.M. and T.B. performed mass-spectrometry measurements. A.M. supervised the project. A.C.F. and A.M. wrote the manuscript.

proteins, MAD2 and BUBR1 (the latter forming a constitutive complex with BUB3) interact directly with CDC20, an APC/C co-activator. The resulting quaternary complex, comprising MAD2, BUBR1:BUB3, and CDC20, represents the core of the mitotic checkpoint complex (MCC^{core}), the SAC effector8–10 (Figure 1a and Extended data Figure 1a-b). MCC^{core} binds APC/C (already bound to a second Cdc20 molecule) and inhibits its activity11–13. Thus, CDC20, an APC/C co-activator when devoid of SAC proteins, becomes an APC/C inhibitor when bound to SAC proteins in MCC.

MAD2 binds the MAD2-interacting motif (MIM) of CDC20. This promotes a striking topological remodelling of MAD2 from an open (O-MAD2) to a closed conformation (C-MAD2) of its “safety belt” or “seatbelt”, a structurally mobile element comprising the last ~45 residues of MAD214,15 (Extended data Figure 1c). Direct measurements indicated that O-MAD2 binds to the CDC20 MIM with a dissociation constant (K_D) of ~10^{-7} M (references 14,15). However, when measured *in vitro*, the reaction appeared to have remarkably small on-rate constant (reference 2–4) likely because MAD2 structural remodelling entails large activation energy. Thus, binding of MAD2 to CDC20 may be rate limiting for SAC activation. Because SAC reactivation requires minutes in cells5–7, this binding reaction is likely catalysed.

To resolve this conundrum, we introduced fluorophores in recombinant human O-MAD2, CDC20, and BUBR1 we created fluorescence resonance energy transfer (FRET) sensors for MCC assembly. MCC Sensor 1 (MCC^{S1} in figures) monitors binding of ^{CFP}CDC20 and O-$MAD2^{TAMRA}$ (Figure 1b and Extended data Figure 2a-c). Sensor 2 (MCC^{S2}) monitors binding of ^{CFP}BUBR1 and O-$MAD2^{TAMRA}$ (Figure 1b and Extended data Figure 2a,d,e). Injected into mitotic HeLa cells, the fluorescent proteins localized to kinetochores, where SAC proteins normally reside during mitosis, showing they are functional (Extended data Figure 3).

We measured the FRET acceptor fluorescence of Sensor 1 at different concentrations of O-MAD2 after a 15-hour pre-incubation, i.e. at equilibrium (Figure 1c, red curve). The dissociation constant of the CDC20:C-MAD2 interaction (K_d = 150 nM) was similar to that previously measured with CDC20 peptides encompassing the MIM motif3,14,15. When we titrated O-MAD2 in presence of dark (i.e. non fluorescently labelled) BUBR1, 3 nM O-MAD2 were sufficient to obtain half-maximal saturation of MCC Sensor 1 [apparent K_d (App. K_d), defined in Supplementary Information, Section A], indicating a strongly augmented (~50-fold) binding affinity (Figure 1c, blue curve).

There was no FRET signal from Sensor 2 in the absence of CDC20, indicating that CDC20 is necessary for high-affinity binding of BUBR1 and O-MAD2 (Extended data Figure 2d). As for Sensor 1, the apparent K_d for binding of O-MAD2 to BUBR1 in presence of CDC20 was 3 nM (Figure 1c, green curve), indicating that the chosen position of fluorophores does not interfere with MCC assembly. Co-elution of the four subunits of MCC Sensor 1 from a size exclusion chromatography (SEC) column further supports this (Extended data Figure 2f).

Removal of BUB3 did not affect the stability of MCC (Extended data Figure 2g). BUBR1 binds CDC20 in MCC^{core} through its first KEN-box (KEN1) motif11 (Extended data Figure 1a), while binding to the second CDC20 subunit (see Introduction) requires KEN2 (reference 11). The CDC20-dependent FRET signal of Sensor 2 requires KEN1, but not KEN2 (Figure 1d; blue and green curves, respectively), showing that Sensor 2 monitors assembly of MCC^{core}. The apparent binding affinity did not change in presence of the KEN2 mutant, suggesting that binding of a second CDC20 does not stabilize MCC^{core}. These studies at equilibrium support important conclusions: 1) MCC^{core} assembly is high-affinity, and therefore BUBR1, CDC20, and O-MAD2, whose cellular concentrations are at least 10 times higher than the apparent K_ds we measured (Supplementary Information, Section B), are expected to associate spontaneously; 2) interactions engaging two MCC subunits are strongly augmented upon addition of the third subunit (e.g. BUBR1 augments CDC20:MAD2 interaction).

We used Sensor 2 for real-time FRET measurements of MCC assembly. The time-dependence of the FRET signal could be fitted with a single exponential function to yield an apparent reaction rate (k_{obs}) that increased linearly with the concentration of MAD2 (Extended data Figure 4a,b), indicative of pseudo-first order kinetics. At a near-physiologic concentration of MCC components (100 nM), MCC assembly measured with Sensor 2 was very slow, with a halftime ($t_{1/2}$) of ~220 min (or 13200 seconds, Figure 2a). Sensor 1 displayed precisely the same slow rates of Sensor 2 (Extended data Figure 4d, red curve). Omission of BUBR1 did not change the rate of activation of Sensor 1 (Extended data Figure 4d, red and blue curves). Instead, when $O\text{-}MAD2^{TAMRA}$ and CDC20 were pre-incubated, and ^{CFP}BUBR1 added to pre-formed CDC20:$C\text{-}MAD2^{TAMRA}$, MCC formed essentially instantaneously (Figure 2a). Thus, reorganization of the MAD2 safety belt upon binding of $O\text{-}MAD2^{TAMRA}$ and ^{CFP}CDC20 may be rate-limiting for MCC^{core} assembly3 and the likely target of the catalytic apparatus of the SAC (Figure 1a).

The MAD1:C-MAD2 complex is the kinetochore receptor of O-MAD2 and has been proposed to accelerate its conversion required for Cdc20 binding via a template-directed mechanism16,17 (the MAD2 template model, see Supplementary Information, Section C). Previous studies, however, detected only modest effects of MAD1:C-MAD2 on MCC assembly *in vitro*, clearly insufficient to account for rapid MCC accumulation in living cells3,4,16. MAD1:C-MAD2 might therefore require an activator, and we focused on the protein kinases BUB1:BUB3 and MPS1 because of their role in the regulation of MAD1:C-MAD2 (reference 1).

We pre-incubated recombinant MAD1:C-MAD2, BUB1:BUB3, and MPS1 at 1 μM for 30 minutes at 30ºC with ATP and Mg^{2+} before diluting them at different concentrations into solutions containing MCC FRET Sensor 2 (Figure 2b). Already at low nanomolar concentrations, pre-incubated MAD1:C-MAD2, BUB1:BUB3, and MPS1 produced strong enhancements of the rate of MCC assembly (Figure 2b). The initial velocity of MCC formation increased linearly as a function of catalyst concentration (Extended data Figure 4e). At concentrations (25-50 nM) comparable to those reported to exist in cells, pre-incubated MAD1:C-MAD2, BUB1:BUB3, and MPS1 caused the MCC binding reaction to equilibrate in minutes ($t_{1/2}$ = 165 and 82 seconds, respectively, Figure 2b), in line with

signalling dynamics *in vivo*5,6. At equivalent concentrations of MCC subunits and catalytic activators, Sensor 1 behaved essentially indistinguishably from Sensor 2 (Extended data Figure 4f). Thus, our *in vitro* assay captures a crucial step of catalytic activation of the SAC.

To identify factors necessary for rapid MCC accumulation, we omitted individual components from the pre-incubation step (catalysts' concentrations in these experiments is discussed in Supplementary Information, Section D). Removing MAD1:C-MAD2 prevented any acceleration of MCC formation (Figure 3a). Removing MPS1 (Figure 3b) or adenosine triphosphate (ATP, Figure 3c) resulted in strong decreases of MCC assembly rate. Removing BUB1:BUB3 had a large but less dramatic effect (Extended Data Figure 5a).

Asymmetric dimerization of O-MAD2 and C-MAD2 has been invoked as part of the mechanism of MAD2 activation in the SAC3,16,17. We asked if MAD2 mutations in the MAD1:C-MAD2 complex that prevent dimerization with O-MAD2 (references 17,18) would ablate the catalytic role of MAD1:C-MAD2. Indeed, MAD1:C-MAD2$^{R133A\text{-}F141A}$ was inert, confirming MAD2 dimerization as a crucial element of the catalytic mechanism (Figure 3d). N-terminal truncations of MAD1 (Extended data Figure 1d and 2a) showed that residues 1-419 of MAD1 are dispensable for catalysis, while further deletions affecting residues 420-485 decreased the catalytic function of MAD1:C-MAD2 (Extended data Figure 5b).

MPS1 and BUB1 are protein kinases. We studied the relevance of kinase activity on the catalytic reaction with the small-molecule inhibitors Reversine and BAY-320, respectively targeting MPS1 and BUB1 (references 19,20; Extended data Figure 6a). Addition of Reversine during pre-incubation had dramatic negative consequence for catalytic activation of MCC assembly, while its addition at the end of pre-incubation was fully compatible with catalysis. Thus, MPS1 activity is only required during pre-incubation (Figure 4a). Much milder effects were observed with BAY-320, suggesting that BUB1 kinase activity has relatively modest effects on catalytic activation of MCC (Extended data Figure 6b).

We dissected the requirements for kinase activity by performing separate pre-incubation reactions (with ATP) with (a) MPS1 and MAD1:C-MAD2, and (b) BUB1:BUB3. Catalysis was fully reconstituted when the two pre-incubation reactions were added to Sensor 2 and CDC20 (Extended data Figure 6c). Addition of Reversine to MPS1 and MAD1:C-MAD2 during pre-incubation strongly reduced the rate of MCC assembly (Extended data Figure 6d), suggesting that MPS1 phosphorylates and activates MAD1:C-MAD2.

By mass spectrometry, we identified several phosphorylation sites on the MAD1:MAD2 complex after *in vitro* phosphorylation with MPS1 (Extended data Figure 7a). Based on sequence conservation, previous phosphoproteomic analyses (as summarized in the PHOSIDA and Phosphosite Plus web sites), and previous functional analyses, we prioritized on four MPS1 phosphorylation sites located in two distinct regions of MAD1: Ser428 (in the coiled-coil region of MAD1, upstream of the MIM), and Ser699, Ser713 and Thr716 [in the RWD domain (RING finger, WD repeat, DEAD-like helicase)] (references 14,15,21) (Extended data Figure 1d and 7a). An alanine point mutant of Ser428 (S428A) had no effect on the catalytic role of MAD1:C-MAD2 (Figure 4b). Conversely, a triple alanine mutant of

Ser699, Ser713 and Thr716 (designated RWD-A) abrogated the catalytic role of MAD1 in MCC assembly. The residual response of MAD1^{RWD-A} was ascribed to the BUB1, because its omission completely abrogated catalysis. Our attempts to generate phospho-mimetic mutants of MAD1:C-MAD2 were frustrated by instability of the protein products (A.F. and A.M., unpublished data).

Removal of MAD1:C-MAD2 from kinetochores following microtubule attachment is required to suppress SAC signalling. A chimeric fusion protein of MAD1 and MIS12 (which stably binds kinetochores) prevents MAD1 release and instates a metaphase arrest22. Indeed, when expressed in HeLa cells, the MIS12-MAD1^{WT} chimera created a durable checkpoint arrest in mitosis, which was suppressed by inhibition of MPS1 with Reversine (Figure 4c and Extended data figure 7b-d). MIS12-MAD1^{S428A} behaved like MIS12-MAD1^{WT}, whereas MIS12-MAD1^{RWD-A} failed to arrest, indicating that the RWD-A mutant impairs the SAC response caused by fusing MAD1 to MIS12 (Figure 4c). Thus, preventing MPS1 phosphorylation with the RWD-A mutant abrogates the catalytic role of MAD1:C-MAD2 *in vitro* as well as in an established SAC assay in human cells.

A 10-fold reduction of the concentration of MPS1 during pre-incubation had very modest effects on the halftime of MCC assembly, suggesting that MPS1 can perform multiple rounds of MAD1:C-MAD2 phosphorylation (Extended data figure 8a, conditions 1 and 4). Conversely, a 10-fold reduction of the concentration of either MAD1:C-MAD2 or BUB1:BUB3 (Extended data figure 8a) resulted in ~3-fold increase of halftimes of MCC accumulation. 10-fold reduction of the concentrations of MAD1:C-MAD2 and BUB1:BUB3 compounded the individual effects, causing a 10-fold reduction of the halftime of MCC accumulation.

These observations suggest that MAD1:C-MAD2 and BUB1:BUB3 may both act as physical constituents of the catalyst of MCC assembly, in line with evidence that these proteins may physically interact (Supplementary Information, Section E). To test this idea, we measured the influence of BUB1:BUB3 on binding of CDC20 and MAD2 with Sensor 1. When BUB1:BUB3 was omitted, strong reduction of CDC20:C-MAD2 complex formation was observed (Extended data figure 8b). This effect did not involve BUBR1:BUB3 (which binds directly to BUB1:BUB3, reference 23), because omission of BUBR1:BUB3 did not influence the rate of FRET accumulation from Sensor 1 (Extended data figure 8b).

We therefore asked if BUB1 exercises its functions through CDC20. Indeed, when using a BUB1 construct with mutations in a CDC20 binding motif, the KEN1-ABBA motif24–26, we observed that the rate of assembly of CDC20:C-MAD2 was reduced to levels similar to those observed after removing BUB1:BUB3 (Extended data figure 8c). Thus, the contribution of BUB1 to MCC assembly appears to require an interaction with CDC20, and we surmise that kinase activity of BUB1 mildly stimulates this interaction.

MAD1 and BUB1 have been previously shown to interact27–29. We therefore asked if human MAD1:C-MAD2 and BUB1 form a complex by performing pull-down experiments in which MBP-MAD1:C-MAD2 was immobilized on amylose beads (Extended data figure 8d). We observed binding of BUB1:BUB3 to MBP-MAD1:C-MAD2 only in the presence of

MPS1 kinase activity, suggesting that MPS1 triggers the interaction, like in *Saccharomyces cerevisiae*27. The interaction of MAD1:C-MAD2 and BUB1:BUB3 is transient and low affinity, as the proteins did not co-elute from a SEC column (unpublished results).

Our data indicate that BUB1:BUB3 and MAD1:C-MAD2 (the latter after appropriate modification by MPS1) accelerate the conversion of O-MAD2 required to bind CDC20. Our hypothesis is that MPS1, MAD1:C-MAD2, and BUB1:BUB3 act strictly catalytically, i.e. they do not effect changes in the free energy of association of the MCC subunits. To test this, we asked if the K_d of MCC^{S2} (already shown in Figure 1c) changed when measured in the presence of catalysts (at 25 nM) at equilibrium. In agreement with our hypothesis, the presence of catalysts did not change the apparent binding affinity of MCC^{S2} (Extended data figure 8e). Michaelis-Menten parameters K_M and k_{cat} calculated by fitting initial velocities at varying concentrations of MAD2 indicated considerable efficiency of the SAC catalyst (k_{cat}/K_M in excess of 10^5 s^{-1} M^{-1}, Figure 5a).

Here, we have shown that the conversion of O-MAD2 required for binding CDC20 is the only rate-limiting step for MCC assembly. MAD2 is not a mere catalyst for the interaction of BUBR1 and CDC20 as proposed4,30. Rather, it binds BUBR1 and CDC20 in a stable ternary complex that assembles spontaneously at the cellular concentration of SAC proteins. A crucial implication of this biochemical design is that disassembly of MCC requires energy. Several energy-utilizing mechanisms of MCC disassembly have been described and shown to operate continuously to disassemble MCC even when the rate of MCC assembly is maximal31.

We identify a phosphorylated form of MAD1:C-MAD2 as the crucial catalyst for the accumulation of CDC20:C-MAD2. Omission of MPS1 and usage of a truncated and partly inactive MAD1 construct likely explain why previous studies observed very modest catalytic activation of MAD2 *in vitro*3 (see Supplementary Information, Section F) Our results also indicate that dimerization of O-MAD2 with MAD1:C-MAD2, previously shown to be required for SAC signalling16,32, is essential for catalysis. Two crucial predictions of the MAD2 template model, that MAD1:C-MAD2 is a catalyst, and that O-MAD2:C-MAD2 dimerization is required for catalysis16, are therefore demonstrated here (Figure 5b,c).

Kinetochores are likely required for a robust SAC response, in particular by increasing the local concentration of catalysts, favouring their post-translational modifications and physical interactions. The role of kinetochores in SAC signalling may be particularly important under stringent conditions such as the presence of a few or a single unattached kinetochore in a cell33, when the levels of MCC decline and the rate of degradation of APC/C substrates raises considerably5,34. The tools we described here may enable the study of this important and unresolved question.

Methods

Production of recombinant proteins

All recombinant proteins used in this study were of human origin. MAD2 was expressed and purified essential as described before17. All proteins used in this study, except BUBR1

(residues 1 to 571), were full length. To generate fluorescent BUBR1 and CDC20, we introduced a his-tagged N-terminal mTurquoise2 (reference 35). Expression of all other protein constructs and mutants were done in Sf9 (CDC20 and BUB1:BUB3) or TnaO38 insect cells (all other proteins). After infection with virus (1:50), cultures were grown at 27ºC degrees and harvested after three days, and pellets stored at -20ºC. MAD1:C-MAD2 and BUBR1:BUB3 were cultured by mixing individual viruses, each harboring individual genes. MPS1 was expressed in the presence of 2 μM Reversine.

Generally, cells were lysed in Buffer A (25 mM Hepes (pH 7.5), 300 mM NaCl, 10 % glycerol, 2 mM TCEP, 1 mM PMSF). MAD1:C-MAD2 and CDC20 were purified in Buffer A with 1000 and 500 mM NaCl, respectively. Soluble lysate was passed over a 5ml Ni-NTA column, and after washing with 20 CV Buffer A, the proteins were eluted by adding 300 mM imidazole to Buffer A. Proteins was subsequently gel filtered on a Superdex S200 16/60 column equilibrated against Buffer B (10 mM Hepes (pH 7.5), 150 mM NaCl, 5 % glycerol, 2 mM TCEP). All buffers of the MPS1 purification were supplemented with 0.2% Triton X-100. Fractions containing purified proteins were concentrated, flash frozen and stored at -80 degrees Celsius until use.

TAMRA-labeling of O-MAD2

Purified MAD2 was C-terminally labeled using the sortase A transpeptidase enzyme from *Staphylococcus aureus*, which catalyzes the cleavage of a short 5 amino acid recognition sequence (LPETG) with the concomitant formation of an amide linkage between an oligoglycine peptide and the target protein36. To that end, we mixed between 10 to 50 μM of MAD2-LPETG with 150 μM SortaseA and 0.5 to 1 mM of a TAMRA-conjugated peptide (GlyGlyGlyGlyLys-TAMRA, StorkBio, Estonia). The reactants were mixed in 50 mM Tris-HCL (pH 7.5), 150 mM NaCl and 10 mM $CaCl_2$ and incubated overnight at 4 °C. In order to purify MAD2 in the open conformation (O-MAD2), the labeling reaction was followed by an ion exchange (ResQ column, GE Healthcare) to remove the SortaseA, excess TAMRA-conjugated peptide and MAD2 in the closed conformation (C-MAD2).

FRET measurements

Fluorimeter scans were performed on a Fluoromax 4 (Jobin Yvon) in a buffer containing fresh 10 mM Hepes (pH 7.5), 150 mM NaCl, 2.5 % glycerol, 10 mM beta-mercaptoenthanol and 0.05% triton X-100. Mixtures were excited at 430 nm and the emissions were scanned from 450 to 650 nm. Single wavelength acceptor fluorescence measurements were carried out at 583 nm. Mixtures of MAD1:C-MAD2 with BUB1:BUB3 and/or MPS1 were pre-incubated at 1 μM for 30 min at 30 degrees. Unless stated otherwise, assays were performed using 100 nM of all proteins, except CDC20, which was added at 500 nM. In all panels reporting time-dependent changes in FRET signal of Sensors 1 and 2, curves report single measurements representative of at least three independent technical replicates.

Kinetic analysis MCC catalysis

To determine the kinetic parameters for catalysis of MCC assembly, we measured initial rates of catalysis of 5 nM ‘enzyme’ (MAD1:MAD2, BUB1:BUB3 and MPS1, which were pre-activated by incubation for 30 minutes at 30ºC with 1 mM ATP/$MgCl_2$ at 1 μM) against

500 nM CDC20 and BUBR1, while the concentration of MAD2-TAMRA was varied. The initial rates of MCC assembly were calculated using a standard of fluorescence emission at 583 nm at known MCC concentrations. The initial rates were subsequently plotted against the concentration of MAD2, and subjected to non-linear regression fitting using the Michaelis-Menten equation $V = (V_{max} \times [MAD2])/([MAD2] + K_M)$, where V_{max} is the maximal velocity at saturating substrate concentrations and K_M is the Michaelis-Menten constant. The k_{cat} value was derived from the equation $k_{cat} = V_{max}/[E_0]$, where E_0 is the total enzyme concentration. Experimental data was processed using Prism 6 (Graphpad Software, Inc.). Fluorimeter scans were performed on a Fluoromax 4 (Jobin Yvon) in a buffer containing fresh 10 mM Hepes (pH 7.5), 150 mM NaCl, 2.5 % glycerol, 10 mM beta-mercaptoenthanol and 0.05% triton X-100. Mixtures were excited at 430 nm and the emissions were measured at 583 nm.

MAD1:C-MAD2 and BUB1:BUB3 pull-down experiments

MBP-MAD1:C-MAD2 (1 μM), BUB1:BUB3 (2 μM), MPS1 (400 nM) and ATP (or variations thereof as described) were incubated for 1 hour at room temperature in 1X kinase buffer (20 mM HEPES pH 7.5, 50 mM NaCl, 10 mM $MgCl_2$, 0.5 mM EGTA, 2 mM DTE, 0.01% Triton). After incubation (30 min on ice) with equilibrated amylose beads (New England Biolabs), the beads were washed with 2 times 200 μl wash buffer (50 mM HEPES pH 7.5, 50 mM NaCl, 0.05% Triton, 10% glycerol, 2 mM DTE). Wash twice with wash buffer, add SDS-loading buffer, boil, and analyze samples by WB.

Mass spectrometry

Liquid chromatography coupled with mass spectrometry was used to identify phosphorylation sites. Samples were digested with LysC/Trypsin and/or GluC and prepared for LC-MS/MS analysis37. 100 ng of peptides were separated on a Thermo Scientific™ EASY-nLC 1000 HPLC system (Thermo Fisher Scientific™, Odense, Denmark; one hour gradient from 5-60% acetonitrile with 0.1% formic acid) and directly sprayed via a nano-electrospray source in a quadrupole Orbitrap mass spectrometer (Q Exactive™, Thermo Fisher Scientific™) (reference 38). The Q Exactive™ was operated in data-dependent mode acquiring one survey scan and subsequently ten MS/MS scans39. Resulting raw files were processed with the MaxQuant software (version 1.5.2.18) using a reduced database containing only the proteins of interest for the search and giving phosphorylation on serine, threonine and tyrosine as variable modification40. A false discovery rate cut off of 1% was applied at the peptide and protein levels and the phosphorylation site decoy fraction.

Cell culture, plasmid transfection, microinjections, immunofluorescences, immunoblotting and imaging

HeLa cells or N-terminally tagged LAP-BUB1 HeLa cells (MCB 2334; a kind gift from A. Hyman) were grown in Dulbecco's Modified Eagle's Medium (DMEM; PAN Biotech) supplemented with 10 % tetracycline-free FBS (PAN Biotech), L-Glutamine (PAN Biotech) and with either penicillin and streptomycin or G418 (GIBCO). Cells were grown at 37°C in the presence of 5 % CO_2. Cdk1 inhibiton, microinjections and live imaging were performed in complemented CO2-independent media (GIBCO) at 37°C. For microinjections, a cDNA segment encoding human CENP-A was cloned in a pcDNA5/FRT/TO-IRES-mCherry

vector, a modified version of pcDNA5/FRT/TO (Invitrogen) generated in house as a C-terminal fusion to mCherry (Marta Mattiuzzo and Anna De Antoni). Transient transfections of pcDNA5/FRT/TO-IRES-mCherry-CENPA were performed with Lipofectamine2000 (Invitrogen) according to the manufacturer's instructions and the mCherry-CENPA fusion was expressed by addition of 200 ng/ml doxycycline (Sigma) for 48 hours. Where indicated, Nocodazole (Sigma) was used at 3.3 μM and RO-3306 (Calbiochem) was used at 9 μM for 18 hours. Microinjections were performed using a combination of FemtoJet, InjectMan-NI2 and Femtotip-II, all purchased by Eppendorf. Recombinant CFP-BUBR1:BUB3 complex and MAD2-TAMRA (or TAMRA) were injected at a concentration of 6μM and 2μM respectively. N (Number of cells injected): for TAMRA N=2; for MAD2-TAMRA N=9; for CFP-BUBR1:BUB3 N=8. Live-cell images were taken before injection and 1 to 10 minutes after injection.

Plasmid expressing mCherry-MIS12-MAD1^{WT} was a kind gift from T. Kapoor. The same plasmid background was used to transiently express a synthetically synthesized *MAD1* gene harboring the various Alanine-mutations. For this assay, HeLa cells growing on coverslips pre-coated with 15 μg/ml poly-D-Lysine (Millipore) were transiently transfected with the mCherry fusions using Lipofectamine 2000 and then, 30 hours after transfection were either prepared for immunofluorescence or processed for western blotting analysis. Were indicated, cells were treated with 500 nM Reversine for 2 hours before fixation. Cells were then fixed with PBS/ Paraformaldehyde 4 % followed by permeabilisation with PBS/PHEM-Tween 0.3 %. The following antibodies were used for immunostaining: anti-α-tubulin (mouse, DM1αSigma; 1:500), anti-CREST/anti-centromere antibodies (human, Antibodies Inc.; 1:100). DNA was stained with 0.5 μg/ml DAPI (Serva) and coverslips mounted with Mowiol mounting media (Calbiochem). For western blotting analysis the following antibodies were used: anti-α-tubulin (DM1α;1/10000), anti-MAD1 (in house made mouse monoclonal, clone BB3-8/e578-589; 1/100). Imaging for microinjection experiments was performed on a spinning disk confocal microscope of a 3i Marianas™ system (Intelligent Imaging Innovations, Denver, CO, USA) equipped with an Axio Observer Z1 microscope (Zeiss, Germany), a CSU-X1 confocal scanner unit (Yokogawa Electric Corporation, Japan), Plan-Apochromat 63x or 100x/1.4NA objectives (Zeiss) and Orca Flash 4.0 sCMOS Camera (Hamamatsu, Japan). Images were acquired as Z-sections (using Slidebook Software 5.5 from Intelligent Imaging Innovations or using LCS 3D software from Leica) and converted into maximal intensity projections TIFF files for illustrative purposes. The imaging for the mCherry fusions experiments was performed on a Deltavision Elite System (GE Healthcare, UK) equipped with an IX-71 inverted microscope (Olympus, Japan), a UPlanFLN 40x/1.3NA objective (Olympus) and a pco.edge sCMOS camera (PCO-TECH Inc., USA). Images were acquired as Z-sections (using the softWoRx software from Deltavision) and converted into maximal intensity projections TIFF files for illustrative purposes. Quantification of kinetochore signals was performed on unmodified Z-series images using Imaris 7.3.4 software (Bitplane). Following background subtraction, a ratio for mCherry-MIS12-MAD1/CREST intensity signals was calculated. All ratios were normalized to the mean of mCherry-MIS12-MAD1^{WT} ratio. The HeLa cell line used in this study was regularly checked for mycoplasma contamination. The cell line was not authenticated.

Europe PMC Funders Author Manuscripts

Data availability statement

The data that support the findings of this study are available from the corresponding author upon request. All uncropped Coomassie-stained gels and Western blots are provided as Supplementary Information.

Extended Data

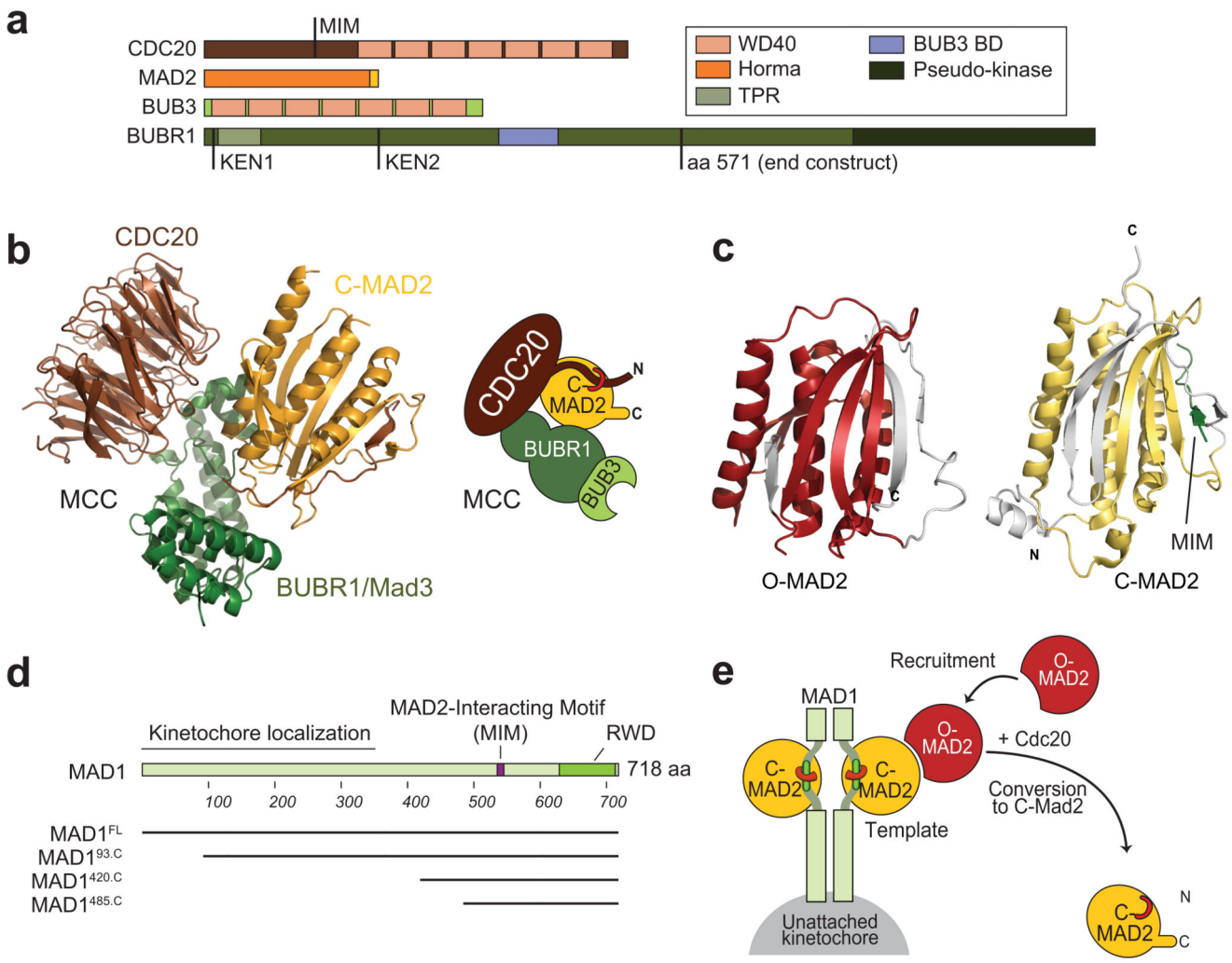

Extended Data Figure 1. MCC constituents and MAD2-template model

a, Schematic of MCC constituents with their domain structure. **b**, Cartoon model of the crystal structure of the *S. pombe* MCC complex[77] (PDB: 4AEZ). CDC20 consists mainly of WD40 β-propeller domain, where the N-terminal extension interacts with MAD2 (MIM). Mad3 is the yeast ortholog of BUBR1. BUBR1, which is constitutively bound to BUB3, contains many functional motifs and structural domains, a few of which are highlighted in **a**. **c**, cartoon models of the crystal structures of O-MAD2 and C-MAD2. The HORMA domain of MAD2 exists in two distinct topologies, 'open' (O-MAD2) when unliganded, and 'closed' (C-MAD2) when bound to MIMs of MAD1 or CDC20 (references 14,15). The

change in topology is due to relocation of mobile elements of the structure, indicated in grey. **d**, Schematic representation of MAD1 and deletion mutants used in this study. **e**, Schematic representation of the MAD2 template model.

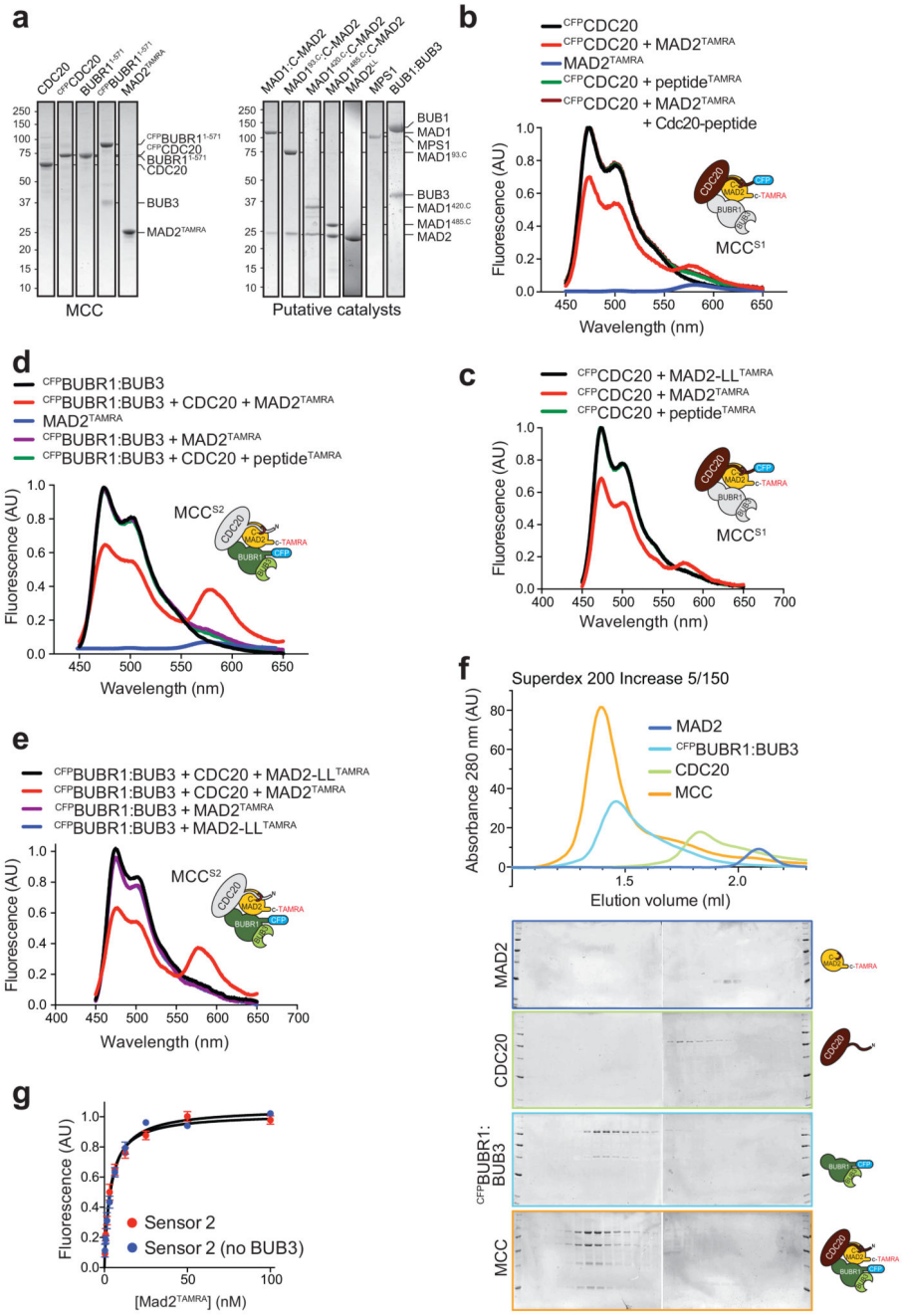

Extended Data Figure 2. Characterizing MCC complex using FRET sensors

a, Coomassie-stained SDS-PAGE of recombinant proteins used in this study. **b**, Fluorescence emission spectrum of MCC Sensor 1 excited at 430 nm. The concentration of all proteins is 100 nM, expect for the CDC20-peptide, which was used in large excess (5

μM) in competition reaction. Signals were normalized to peak donor emission at 470 nm. No change in emission was observed in presence of only $MAD2^{TAMRA}$, or when $^{CFP}CDC20$ was measured in isolation (black) or with a TAMRA-labeled peptide (green). Excess of CDC20-peptide competed for MAD2 binding and no FRET was observed (brown). **c**, In an additional control for Sensor 1, CFP-Cdc20 was tested against TAMRA-labeled "loopless" (MAD2-LL^{TAMRA}), a MAD2 mutant that is locked in the O-MAD2 conformation and that cannot bind CDC20 (reference 17). Assay conditions were as described in panel b. **d**, MCC formation critically relies on the presence of CDC20. Fluorescence emission spectra of MCC Sensor 2 or parts thereof excited at 430 nm. No change in emission was observed in presence of only $MAD2^{TAMRA}$ (no ^{CFP}BUBR1:BUB3, blue) or when ^{CFP}BUBR1:BUB3 was measured in isolation (black), in presence of $MAD2^{TAMRA}$ (without CDC20, purple), or in presence of CDC20 and a TAMRA-labeled peptide not conjugated to MAD2 (green). The only condition leading to changes in donor and acceptor emission was when ^{CFP}BUBR1:BUB3, $MAD2^{TAMRA}$, and CDC20 were present at the same time (red). FRET efficiency upon complex formation at equilibrium was 35%. The concentration of all proteins was 100 nM. Signals were normalized to peak donor emission at 470 nm. **e**, In an additional control for Sensor 2, CFP-BUBR1 was tested in the presence of CDC20 against MAD2-LL^{TAMRA}. Assay conditions were as described in panel d. **f**, Recombinant $MAD2^{TAMRA}$, CDC20 and ^{CFP}BUBR1:BUB3 form MCC complex. Size-exclusion chromatography elution profiles of ^{TAMRA}MAD2 (dark blue trace), CDC20 (green trace), ^{CFP}BUBR1:BUB3 (light blue trace) mixed to form MCC complex (orange trace). Shift in the elution profile indicate complex formation. **g**, BUB3 does not affect MCC core stability. Titration experiment determining the binding isotherms of the MCC complex using sensor 2 in presence (red) or absence (blue) of BUB3 showed indistinguishable apparent K_d's. Bars indicate ± SEM of 3 independent technical replicates of the experiments.

Europe PMC Funders Author Manuscripts

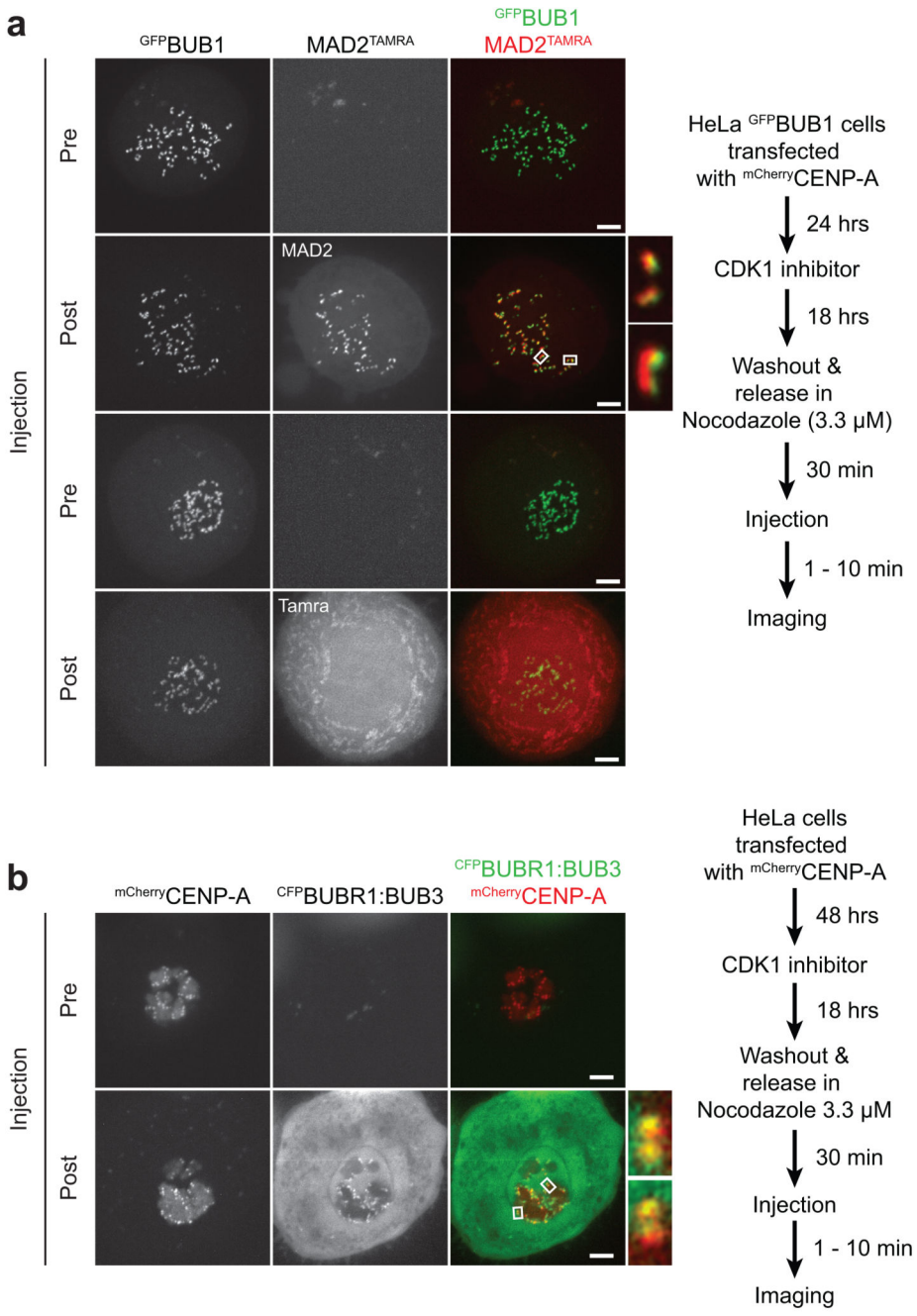

Extended Data Figure 3. Microinjection of recombinant fluorescent MCC proteins

a,b, Recombinant fluorescent MCC proteins inject into mitotic cells localize to kinetochores. HeLa cells constitutively expressing LAP-BUB1 (a) or transiently expressing mCherry-CENP-A (b) were synchronized in the G2 phase of the cell cycle by treatment with the CDK1 inhibitor RO3306 (reference 80) and released into mitosis in the presence of Nocodazole. Shortly after the release, cells were injected with either TAMRA-MAD2 or TAMRA (a), and with CFP-BUBR1:BUB3 (b). Cells were live-imaged both before (Pre) and

after (Post) microinjection. Scale bars = 2 μm. Number of Injected cells, N: for TAMRA N=2; for TAMRA-MAD2 N=9; for Turquoise-BUBR1:BUB3 N=8.

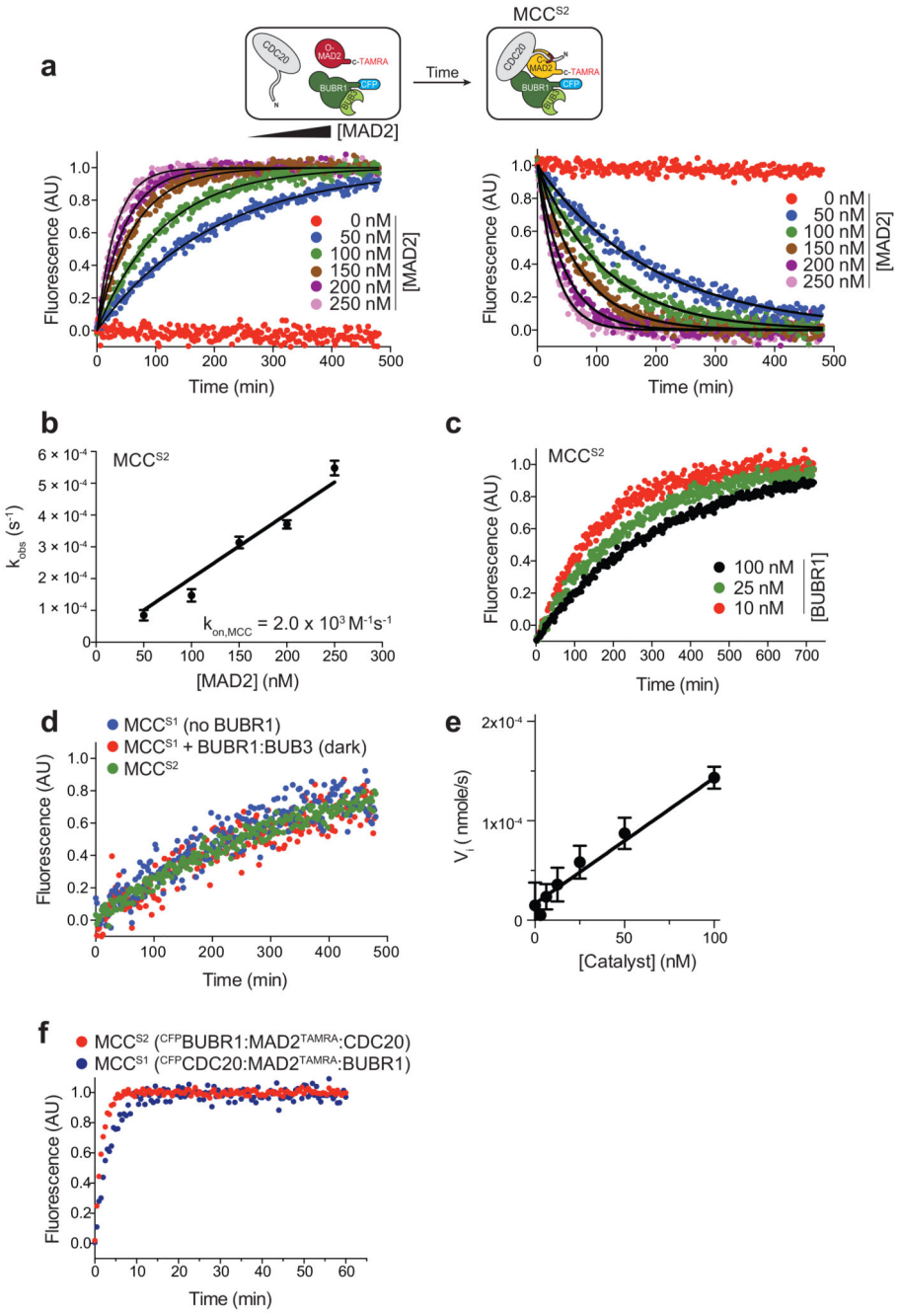

Extended Data Figure 4. MCC assembly kinetics

a, The CDC20:MAD2 complex forms slowly. The time-dependent change of acceptor (left) and donor (right) fluorescence (normalized to values at equilibrium) with 10 nM ^{CFP}BUBR1:BUB3 (see Supplementary Information, Section G on effects of BUBR1 concentration on reaction rate of Sensor 2) and 500 nM CDC20 with varying concentrations

of MAD2^{TAMRA}. Signal changes were fitted to single exponential curves. **b,** After single exponential fitting of the curves in **a**, the apparent first order rate constants (k_{obs}) were plotted as function of MAD2 concentration, with k_{on} being the slope of the resulting curve. These k_{on} values depend on the BUBR1 concentration (see panel **c** and Supplementary Information, Section G). Bars indicate ± SEM of 3 independent technical replicates of the experiments. **c,** MCC assembly assay performed with Sensor 2 at 100 nM MAD2^{TAMRA}, 500 nM CDC20, and the indicated concentrations of ^{CFP}BUBR1:BUB3. **d,** BUBR1 does not influence the assembly kinetics of the MCC. Monitoring the assembly of CDC20:MAD2 (Sensor 1; blue), CDC20:MAD2 with dark BUBR1:BUB3 (Sensor 1; red) and BUBR1:MAD2 with dark CDC20 (green) shows indistinguishable rates. **e,** Catalysis rates scale linearly with catalysts concentration. After pre-incubation of catalyst proteins, MCC assembly was monitored with Sensor 2 [sensor concentrations were 100 nM, except CDC20 (500 nM)] at varying catalyst concentration. Initial velocity (V_i) signal changes were plotted against catalyst concentration, revealing a linear dependency. Bars indicate ± SEM of 3 independent technical replicates of the experiment. **f**, Catalysis of MCC formation could be observed with both FRET sensors. After pre-incubation of MAD1:C-MAD2, BUB1:BUB3 and MPS1 at 1 μM for 30 minutes, similar catalysis rates were observed with either FRET Sensor 1 (blue) or FRET Sensor 2 (red). Assay performed as described in Figure 2b with all proteins at 100 nM.

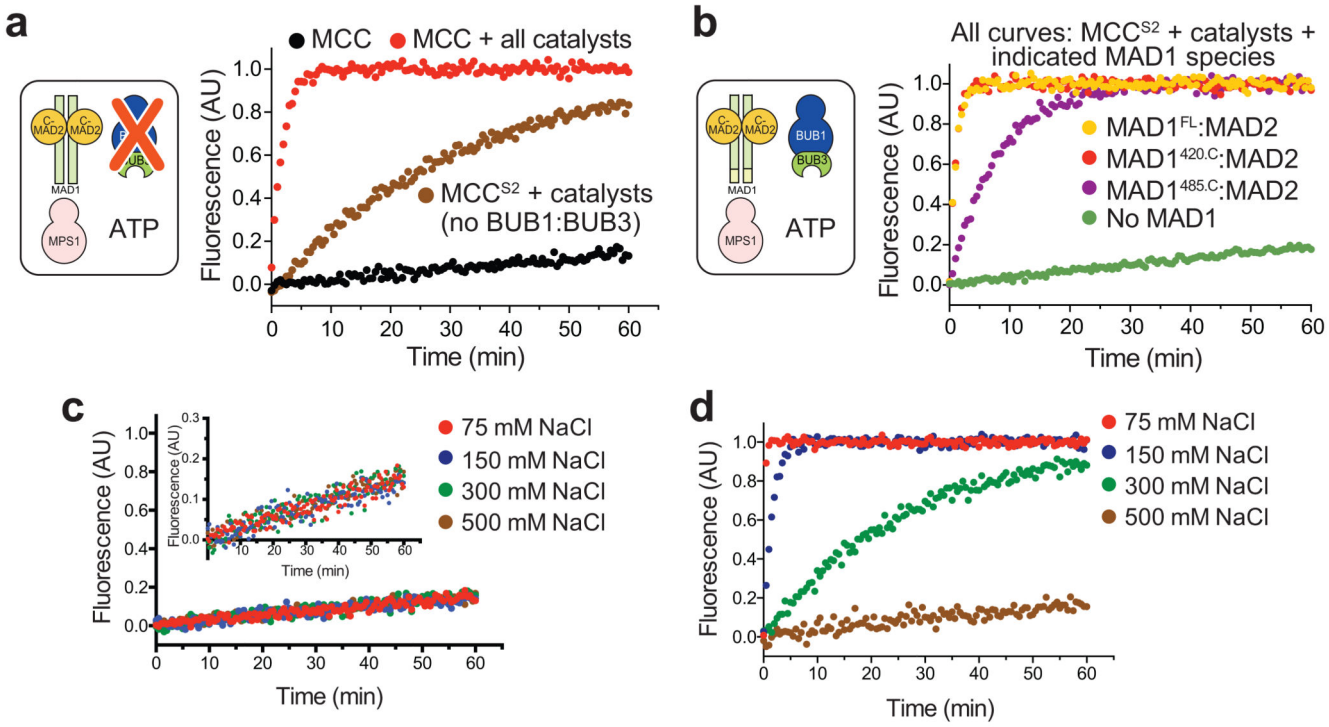

Extended Data Figure 5. Molecular requirements of catalytic MCC assembly

a, catalytic MCC assembly requires MAD1:C-MAD2, MPS1, ATP, and BUB1:BUB3. MCC assembly was monitored with Sensor 2 as described in Figure 2b using 100 nM catalysts. Individual components were omitted as indicated. The same control profiles (black and red

curves) are shown in all panels. **b**, MAD1$^{420\text{-}C}$ (red) is minimal construct capable of full catalysis. Reduction of catalytic rate was observed with MAD1$^{485\text{-}C}$ (purple) compared to MAD1^{FL} (yellow) or MAD1$^{420\text{-}C}$. Assay performed with sensor 2 as described in Figure 2b using 100 nM catalysts. Catalytic activation is salt sensitive, likely because high salt inhibits phosphorylation-mediated polar interactions (Extended data Figure 5c,d). **c-d**, Catalysis is sensitive to salt concentration. MCC assembly was monitored with FRET sensor 2 using either 75 mM (red), 150 mM (blue), 300 mM (green) or 500 mM NaCl (brown), both in the absence (c) or presence (d) of catalysts. Assay performed with Sensor 2 as described in Figure 2b.

Europe PMC Funders Author Manuscripts

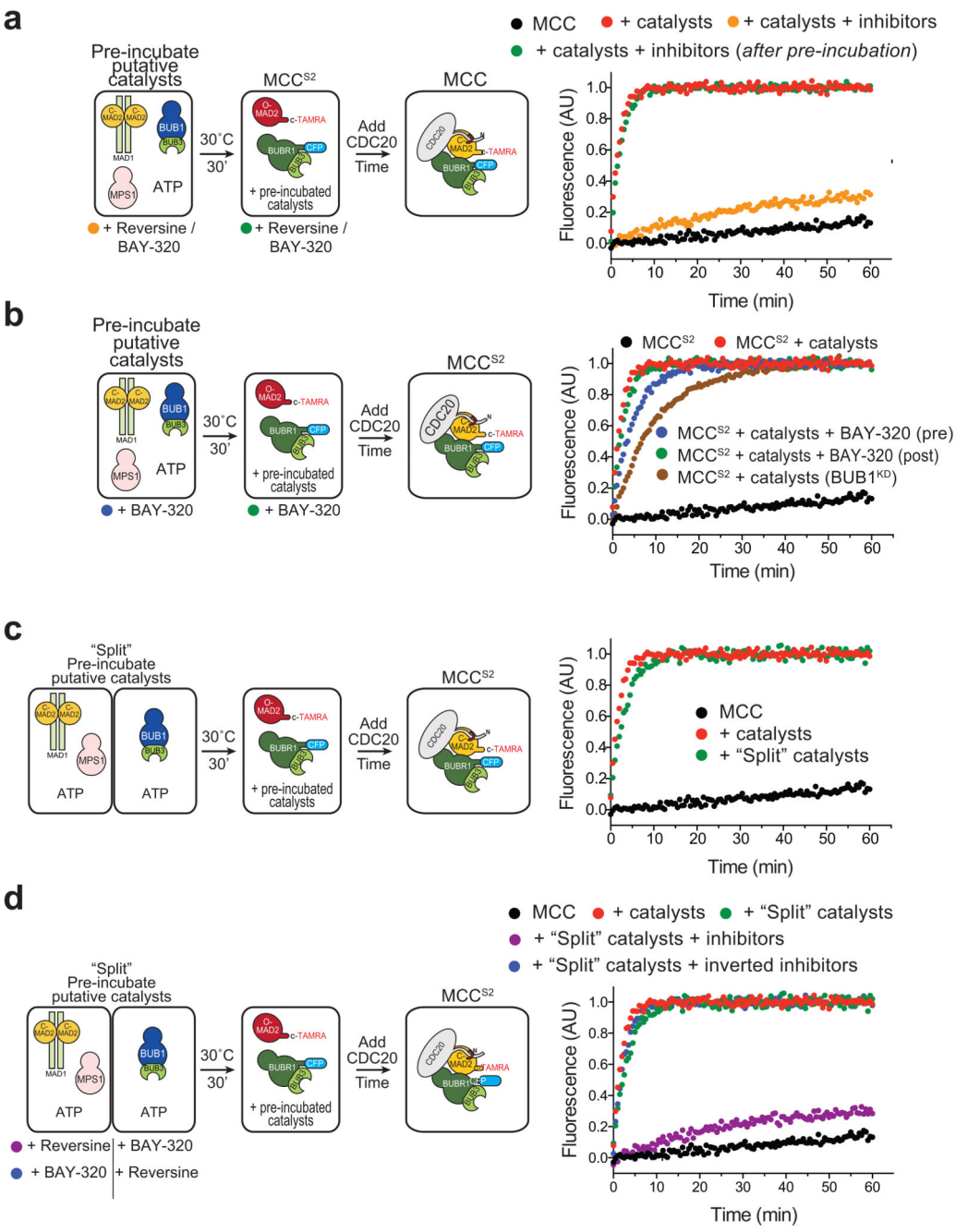

Extended Data Figure 6. Inhibiting catalysis

a, MPS1 and BUB1 inhibition during pre-incubation strongly reduces catalysis. Adding both Reversine and BAY-320 to pre-incubation of catalyst strongly reduced the catalysis of MCC formation. Adding the inhibitors after pre-incubation but before addition to the MCC FRET Sensor 2 components did not affect catalysis. Final concentrations of inhibitors were 50 μM during pre-incubation and 5 μM in assay. **b**, As in Figure 4a, but with BUB1 inhibitor BAY-320. Kinase dead BUB1 ($BUB1^{KD}$) was used as control. **c**, Catalysis rates remained unchanged when "splitting" the pre-incubation of catalyst proteins into two reactions

Europe PMC Funders Author Manuscripts

(MAD1:C-MAD2 together with MPS1 and BUB1 alone; compare green to red). Assay performed with Sensor 2 as described in Figure 2b using 100 nM catalysts. **d,** MAD1:C-MAD2 is phosphorylated by MPS1. Catalysis rates remained unchanged when “splitting” the pre-incubation of catalyst proteins into two reactions (MAD1:C-MAD2 together with MPS1 and BUB1 alone; compare green to red). Adding kinase inhibitors Reversine (MPS1) and BAY-320 (BUB1) to the proper pre-incubation reaction strongly reduced the catalysis rates (orange). However, inverting the inhibitors had no effect on the catalysis rates (blue). Assay performed with Sensor 2 as described in Figure 2b using 100 nM catalysts. Final concentrations of inhibitors are 5 μM in assay (50 μM during pre-incubation).

Europe PMC Funders Author Manuscripts

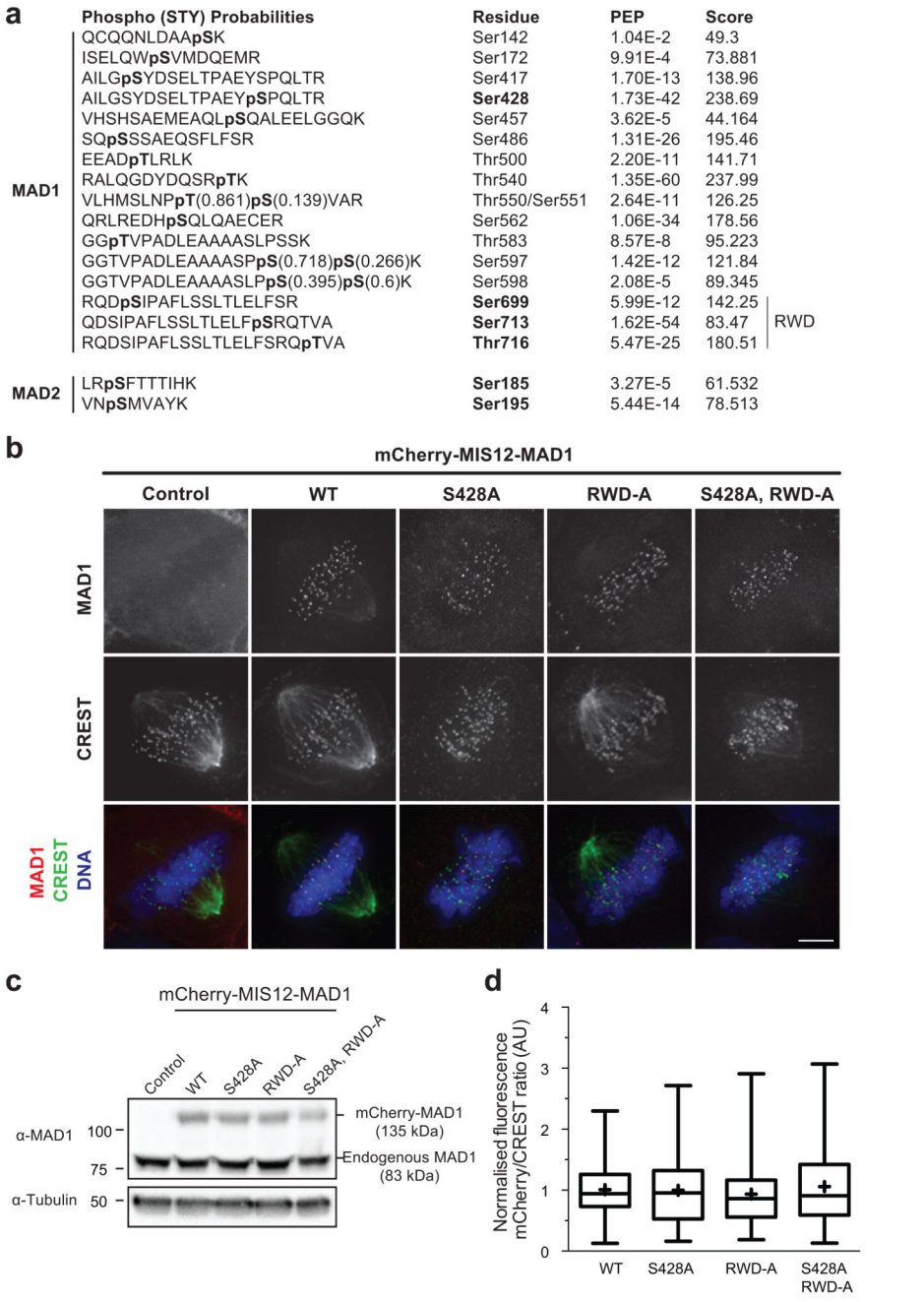

Extended Data Figure 7. MPS1 phosphorylation of MAD1

a, Phosphorylation sites of MAD1 by MPS1. The peptide sequence with the phosphorylated residue in bold, the amino acid position within the protein, the p-value of the posterior error probability for the identified peptide (PEP) and the Andromeda search engine score (score) are shown. Residue numbers in bold indicate phosphorylation sites found in at least two experiments. **b-d,** In (b), HeLa cells were transfected with mCherry (Control), mCherry-MIS12-MAD1^{WT} (WT), mCherry-MIS12-MAD1^{S428A} (S428A), mCherry-MIS12-MAD1^{RWD-A} (RWD-A) or mCherry-MIS12-MAD1$^{S428A,RWD-A}$ (S428A, RWD-A) as

described and quantified in the legend to Figure 4c. Shown are mitotic cells, representative of the mitotic population in each cohort [mCherry control, 59 cells; mCherry-MIS12-MAD1^{WT} (WT), 247 cells; mCherry-MIS12-MAD1^{S428A} (S428A), 203 cells; mCherry-MIS12-MAD1^{RWD-A} (RWD-A), 83 cells; mCherry-MIS12-MAD1$^{S428A,RWD-A}$ (S428A, RWD-A), 91 cells]. Following a 30-hour transfection with the indicated constructs, cells were fixed and processed for western blotting (c) or immunofluorescence (panel d and Figure 4c). Western blot analysis showed that expression levels of mCherry-MIS12-MAD1 fusions are lower than endogenous MAD1 levels (c). Scale bars, 5 μm. Quantification of kinetochore signals was performed on unmodified Z-series images. Following background subtraction, a ratio for mCherry-MIS12-MAD1/CREST intensity signals was calculated. All ratios were normalized to the mean of mCherry-MIS12-MAD1^{WT} ratio. Quantifications are based on two independent biological replicates of the experiment, for a total of 5 cells for each condition, where 254 (WT), 143 (S428A mutant), 207 (RWD-A) or 188 (S428A, RWD-A) kinetochores were analyzed. Shown is a ‘box and whiskers’ graph indicating the median, a box with the 25-75th percentile, and hinges indicating the upper and lower limits of the datapoints.

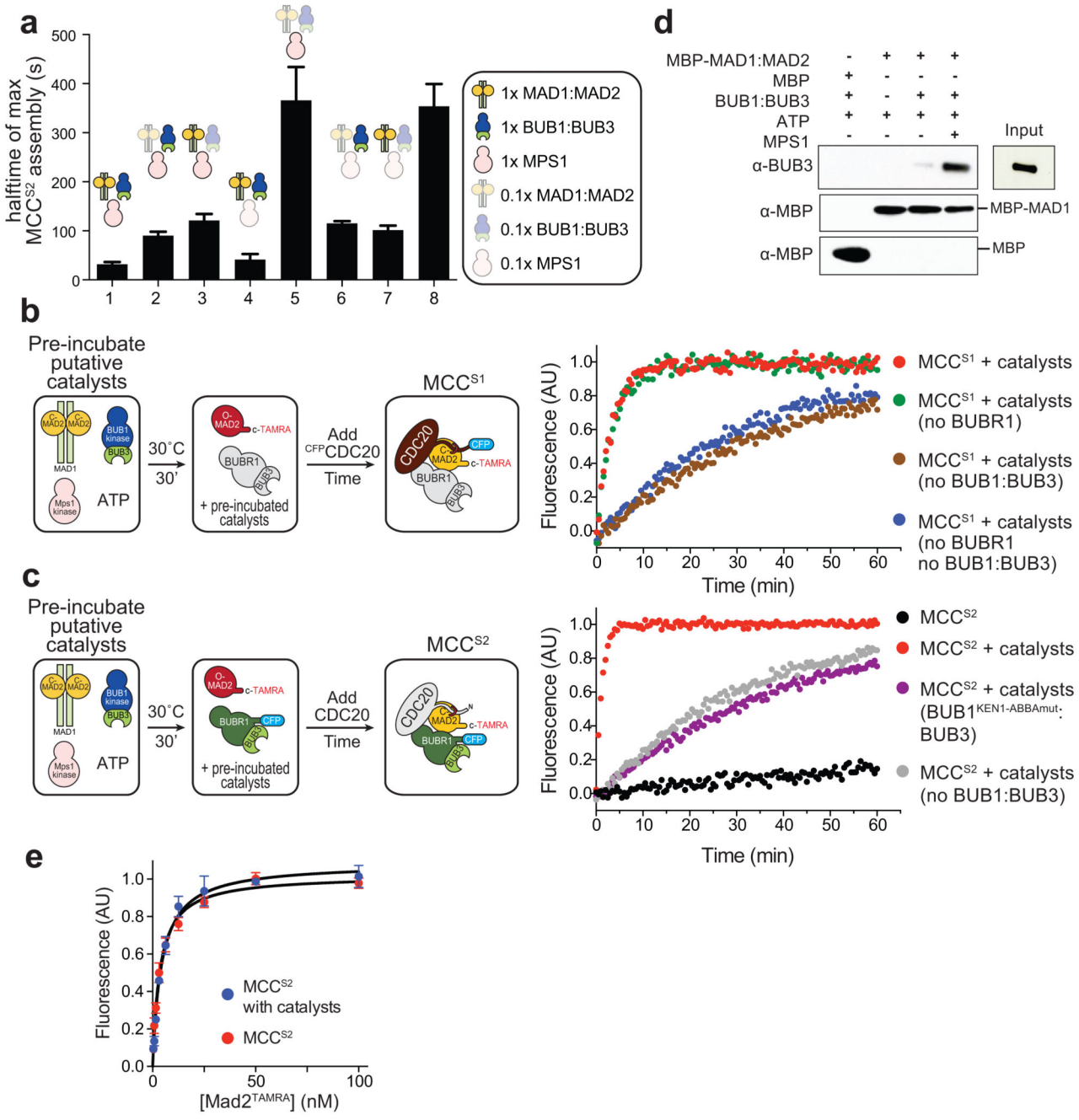

Extended Data Figure 8. MAD1 and BUB1 interact to combine O-MAD2 and CDC20

a, MAD1:C-MAD2 and BUB1:BUB3 together form the MCC enzyme, while MPS1 suffices in sub-stoichiometric amounts. Lowering concentration of all catalysts increased halftime 10-fold (compare conditions 1 and 8). Lowering individual components reduces rates to intermediate levels for MAD1:C-MAD2 (condition 2) and BUB1:BUB3 (conditions 3), but not MPS1 (condition 4). Lowering both MAD1:C-MAD2 and BUB1:BUB3 (condition 5) mimics reduction of all components (condition 8), while reducing MAD1:C-MAD2 or BUB1:BUB3 in combination with MPS1 only resulted in intermediate rates. Assays were

performed with MCC Sensor 2. Bars indicate ± SEM of 3 independent technical replicates of the experiment. Assay performed with sensor 2 and as described in Figure 2b using either 100 nM (1x) or 10 nM (0.1x) catalysts. **b,** Excluding BUBR1 does not affect catalytic rates (green and blue). Assays performed using MCC sensor 1 and all proteins at 100 nM. **c,** BUB1 interaction with CDC20 enhances binding with MAD2. A BUB1 construct that does not bind CDC20 (KEN1-ABBA mutant; purple) yields similar rates as in the absence of BUB1 (grey). Assay performed with sensor 2 and as described in Figure 2b using 100 nM catalysts. **d,** MAD1:C-MAD2 and BUB1:BUB3 show an ATP-dependent interaction in presence of MPS1. Pull-down experiment using MBP-MAD1:C-MAD2 as bait. Assay was performed with 1 μM MAD1:C-MAD2, 2 μM BUB1:BUB3 and 400 nM MPS1. **e**, Values of FRET from MCC Sensor 2 (1 nM ^{CFP}BUBR1 and 500 nM CDC20) after equilibration with or without catalysts (25 nM catalyst concentration). Bars indicate ± SEM of 3 independent technical replicates of the experiment.

Supplementary Material

Refer to Web version on PubMed Central for supplementary material.

Acknowledgements

We are grateful to Tarun Kapoor (Rockefeller University, New York, USA) and Gerhard Siemeister (Bayer Pharma, Berlin) for sharing reagents, Jan-Michael Peters laboratory (IMP, Vienna, Austria) for CDC20 expression vector, Hidde Ploegh (Whitehead Institute for Biomedical Research, Cambridge, USA) for the Sortase expression vector, Yaowen Wu for help with construction of FRET probes, Oliwia Durczak for technical assistance, and Gerben Vader and the Musacchio laboratory for helpful discussions and critical reading of the manuscript. Special thanks to Andrea Ciliberto for precious suggestions and comments. A.C.F. acknowledges support by EMBO long-term fellowship (ALTF 1096-2012) and Marie Curie Intra-European Fellowship (IEF). A.M. acknowledges funding by the Framework Program 7 Integrated Project MitoSys, the Horizon 2020 ERC agreement RECEPIANCE, and the DFG's Collaborative Research Centre (CRC) 1093. The authors declare no competing financial interests.

References

1. Musacchio A. The Molecular Biology of Spindle Assembly Checkpoint Signaling Dynamics. Current biology : CB. 2015; 25:R1002–1018. DOI: 10.1016/j.cub.2015.08.051 [PubMed: 26485365]
2. Luo X, et al. The Mad2 spindle checkpoint protein has two distinct natively folded states. Nature structural & molecular biology. 2004; 11:338–345. DOI: 10.1038/nsmb748
3. Simonetta M, et al. The influence of catalysis on mad2 activation dynamics. PLoS Biol. 2009; 7:e10.doi: 10.1371/journal.pbio.1000010 [PubMed: 19143472]
4. Kulukian A, Han JS, Cleveland DW. Unattached kinetochores catalyze production of an anaphase inhibitor that requires a Mad2 template to prime Cdc20 for BubR1 binding. Developmental cell. 2009; 16:105–117. DOI: 10.1016/j.devcel.2008.11.005 [PubMed: 19154722]
5. Dick AE, Gerlich DW. Kinetic framework of spindle assembly checkpoint signalling. Nature cell biology. 2013; 15:1370–1377. DOI: 10.1038/ncb2842 [PubMed: 24096243]
6. Hagting A, et al. Human securin proteolysis is controlled by the spindle checkpoint and reveals when the APC/C switches from activation by Cdc20 to Cdh1. The Journal of cell biology. 2002; 157:1125–1137. DOI: 10.1083/jcb.200111001 [PubMed: 12070128]
7. Clute P, Pines J. Temporal and spatial control of cyclin B1 destruction in metaphase. Nature cell biology. 1999; 1:82–87. DOI: 10.1038/10049 [PubMed: 10559878]
8. Fraschini R, et al. Bub3 interaction with Mad2, Mad3 and Cdc20 is mediated by WD40 repeats and does not require intact kinetochores. The EMBO journal. 2001; 20:6648–6659. DOI: 10.1093/emboj/20.23.6648 [PubMed: 11726501]

9. Sudakin V, Chan GK, Yen TJ. Checkpoint inhibition of the APC/C in HeLa cells is mediated by a complex of BUBR1, BUB3, CDC20, and MAD2. The Journal of cell biology. 2001; 154:925–936. DOI: 10.1083/jcb.200102093 [PubMed: 11535616]
10. Hardwick KG, Johnston RC, Smith DL, Murray AW. MAD3 encodes a novel component of the spindle checkpoint which interacts with Bub3p, Cdc20p, and Mad2p. The Journal of cell biology. 2000; 148:871–882. [PubMed: 10704439]
11. Izawa D, Pines J. The mitotic checkpoint complex binds a second CDC20 to inhibit active APC/C. Nature. 2015; 517:631–634. DOI: 10.1038/nature13911 [PubMed: 25383541]
12. Alfieri C, et al. Molecular basis of APC/C regulation by the spindle assembly checkpoint. Nature. 2016; 536:431–436. DOI: 10.1038/nature19083 [PubMed: 27509861]
13. Yamaguchi M, et al. Cryo-EM of Mitotic Checkpoint Complex-Bound APC/C Reveals Reciprocal and Conformational Regulation of Ubiquitin Ligation. Molecular cell. 2016; 63:593–607. DOI: 10.1016/j.molcel.2016.07.003 [PubMed: 27522463]
14. Luo X, Tang Z, Rizo J, Yu H. The Mad2 spindle checkpoint protein undergoes similar major conformational changes upon binding to either Mad1 or Cdc20. Molecular cell. 2002; 9:59–71. [PubMed: 11804586]
15. Sironi L, et al. Crystal structure of the tetrameric Mad1-Mad2 core complex: implications of a 'safety belt' binding mechanism for the spindle checkpoint. The EMBO journal. 2002; 21:2496–2506. DOI: 10.1093/emboj/21.10.2496 [PubMed: 12006501]
16. De Antoni A, et al. The Mad1/Mad2 complex as a template for Mad2 activation in the spindle assembly checkpoint. Current biology : CB. 2005; 15:214–225. DOI: 10.1016/j.cub.2005.01.038 [PubMed: 15694304]
17. Mapelli M, Massimiliano L, Santaguida S, Musacchio A. The Mad2 conformational dimer: structure and implications for the spindle assembly checkpoint. Cell. 2007; 131:730–743. DOI: 10.1016/j.cell.2007.08.049 [PubMed: 18022367]
18. Sironi L, et al. Mad2 binding to Mad1 and Cdc20, rather than oligomerization, is required for the spindle checkpoint. The EMBO journal. 2001; 20:6371–6382. DOI: 10.1093/emboj/20.22.6371 [PubMed: 11707408]
19. Santaguida S, Tighe A, D'Alise AM, Taylor SS, Musacchio A. Dissecting the role of MPS1 in chromosome biorientation and the spindle checkpoint through the small molecule inhibitor reversine. The Journal of cell biology. 2010; 190:73–87. DOI: 10.1083/jcb.201001036 [PubMed: 20624901]
20. Baron AP, et al. Probing the catalytic functions of Bub1 kinase using the small molecule inhibitors BAY-320 and BAY-524. Elife. 2016; 5doi: 10.7554/eLife.12187
21. Kim S, Sun H, Tomchick DR, Yu H, Luo X. Structure of human Mad1 C-terminal domain reveals its involvement in kinetochore targeting. Proceedings of the National Academy of Sciences of the United States of America. 2012; 109:6549–6554. DOI: 10.1073/pnas.1118210109 [PubMed: 22493223]
22. Maldonado M, Kapoor TM. Constitutive Mad1 targeting to kinetochores uncouples checkpoint signalling from chromosome biorientation. Nature cell biology. 2011; 13:475–482. DOI: 10.1038/ncb2223 [PubMed: 21394085]
23. Overlack K, et al. A molecular basis for the differential roles of Bub1 and BubR1 in the spindle assembly checkpoint. Elife. 2015; 4:e05269.doi: 10.7554/eLife.05269 [PubMed: 25611342]
24. Di Fiore B, et al. The ABBA motif binds APC/C activators and is shared by APC/C substrates and regulators. Developmental cell. 2015; 32:358–372. DOI: 10.1016/j.devcel.2015.01.003 [PubMed: 25669885]
25. Diaz-Martinez LA, et al. The Cdc20-binding Phe box of the spindle checkpoint protein BubR1 maintains the mitotic checkpoint complex during mitosis. The Journal of biological chemistry. 2015; 290:2431–2443. DOI: 10.1074/jbc.M114.616490 [PubMed: 25505175]
26. Vleugel M, et al. Dissecting the roles of human BUB1 in the spindle assembly checkpoint. Journal of cell science. 2015; doi: 10.1242/jcs.169821
27. London N, Biggins S. Mad1 kinetochore recruitment by Mps1-mediated phosphorylation of Bub1 signals the spindle checkpoint. Genes & development. 2014; 28:140–152. DOI: 10.1101/gad.233700.113 [PubMed: 24402315]

28. Brady DM, Hardwick KG. Complex formation between Mad1p, Bub1p and Bub3p is crucial for spindle checkpoint function. Current biology : CB. 2000; 10:675–678. [PubMed: 10837255]
29. Moyle MW, et al. A Bub1-Mad1 interaction targets the Mad1-Mad2 complex to unattached kinetochores to initiate the spindle checkpoint. The Journal of cell biology. 2014; 204:647–657. DOI: 10.1083/jcb.201311015 [PubMed: 24567362]
30. Han JS, et al. Catalytic assembly of the mitotic checkpoint inhibitor BubR1-Cdc20 by a Mad2-induced functional switch in Cdc20. Molecular cell. 2013; 51:92–104. DOI: 10.1016/j.molcel.2013.05.019 [PubMed: 23791783]
31. Musacchio A, Ciliberto A. The spindle-assembly checkpoint and the beauty of self-destruction. Nature structural & molecular biology. 2012; 19:1059–1061. DOI: 10.1038/nsmb.2429
32. Mapelli M, et al. Determinants of conformational dimerization of Mad2 and its inhibition by p31comet. The EMBO journal. 2006; 25:1273–1284. DOI: 10.1038/sj.emboj.7601033 [PubMed: 16525508]
33. Rieder CL, Cole RW, Khodjakov A, Sluder G. The checkpoint delaying anaphase in response to chromosome monoorientation is mediated by an inhibitory signal produced by unattached kinetochores. The Journal of cell biology. 1995; 130:941–948. [PubMed: 7642709]
34. Collin P, Nashchekina O, Walker R, Pines J. The spindle assembly checkpoint works like a rheostat rather than a toggle switch. Nature cell biology. 2013; 15:1378–1385. DOI: 10.1038/ncb2855 [PubMed: 24096242]
35. Goedhart J, et al. Structure-guided evolution of cyan fluorescent proteins towards a quantum yield of 93%. Nature communications. 2012; 3:751.doi: 10.1038/ncomms1738
36. Popp MW, Ploegh HL. Making and breaking peptide bonds: protein engineering using sortase. Angew Chem Int Ed Engl. 2011; 50:5024–5032. DOI: 10.1002/anie.201008267 [PubMed: 21538739]
37. Rappsilber J, Mann M, Ishihama Y. Protocol for micro-purification, enrichment, pre-fractionation and storage of peptides for proteomics using StageTips. Nat Protoc. 2007; 2:1896–1906. DOI: 10.1038/nprot.2007.261 [PubMed: 17703201]
38. Michalski A, et al. Mass spectrometry-based proteomics using Q Exactive, a high-performance benchtop quadrupole Orbitrap mass spectrometer. Mol Cell Proteomics. 2011; 10:M111 011015.doi: 10.1074/mcp.M111.011015
39. Olsen JV, et al. Higher-energy C-trap dissociation for peptide modification analysis. Nat Methods. 2007; 4:709–712. DOI: 10.1038/nmeth1060 [PubMed: 17721543]
40. Cox J, Mann M. MaxQuant enables high peptide identification rates, individualized p.p.b.-range mass accuracies and proteome-wide protein quantification. Nat Biotechnol. 2008; 26:1367–1372. DOI: 10.1038/nbt.1511 [PubMed: 19029910]

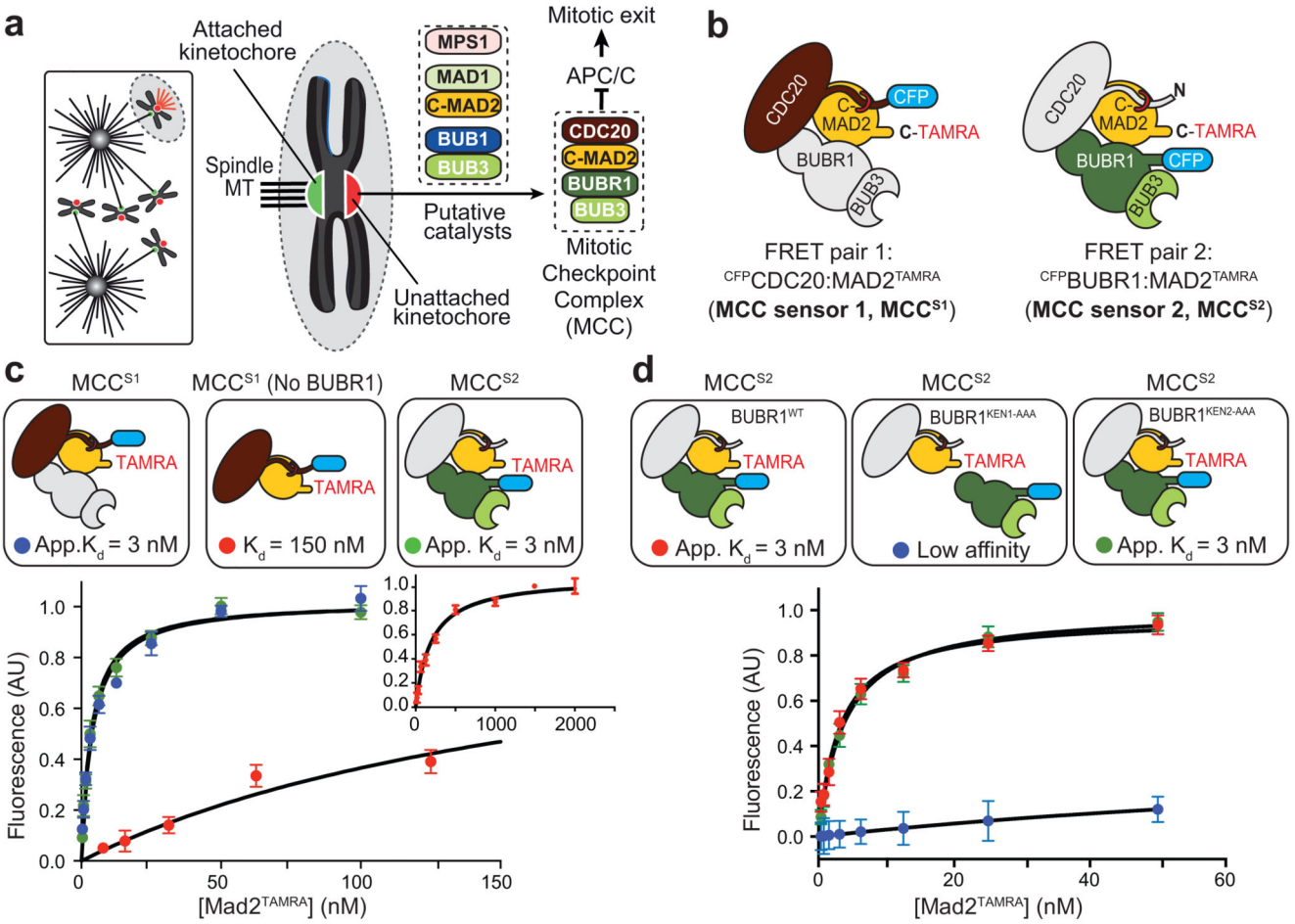

Figure 1. Stability of MCC

a, Putative SAC catalysts at unattached kinetochores promote MCC assembly to inhibit APC/C, preventing mitotic exit. **b**, Scheme of two MCC FRET sensors used. **c**, Intersubunit interactions in MCC augment binding affinity. Response of Sensor 1 and Sensor 2 to the indicated MAD2 concentrations (red, Sensor 1, no BUBR1; Blue, Sensor 1, with BUBR1; Green, Sensor 2). BUBR1 augments the stability of Sensor 1. 1 nM ^{CFP}CDC20, 500 nM BUBR1 (Sensor 1), or 1 nM ^{CFP}BUBR1 and 500 nM CDC20 (Sensor 2) were used. Bars indicate ± SEM of 3 independent technical replicates of the experiment. Unless otherwise specified, “Fluorescence” on the Y-axis indicates FRET acceptor fluorescence at the indicated MAD2 concentration normalized to the maximum FRET acceptor fluorescence at saturating MAD2 concentrations (measured at 583 nm). App. K_d is the apparent K_d. **d**, Titration experiment with BUBR1 wild-type (red) or Ala-Ala-Ala (“AAA”) mutants of KEN-box 1 (blue) or KEN-box 2 (green). Bars indicate ± SEM of 3 independent technical replicates of the experiment.

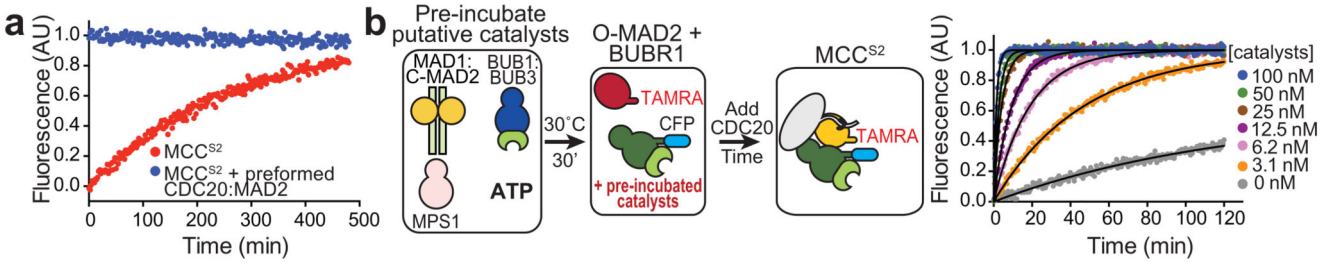

Figure 2. Catalytic assembly of MCC

a, Binding of CDC20 with MAD2 is rate-limiting for MCC formation. Time zero is the first time point after mixing 100 nM ^{CFP}BUBR1:BUB3 with CDC20 and MAD2^{TAMRA} (red) or with CDC20:C-MAD2 allowed to form by overnight pre-incubation at 4ºC (blue). All panels reporting time-dependent changes in FRET signal are single measurements representative of at least three independent technical replicates of the experiment. **b**, MAD1:C-MAD2, BUB1:BUB3 and MPS1 catalyse MCC assembly. After pre-incubation at 30ºC for 30', MAD1:C-MAD2, BUB1:BUB3 and MPS1 were diluted at indicated concentrations into 100 nM MCC FRET Sensor 2 (with 500 nM CDC20).

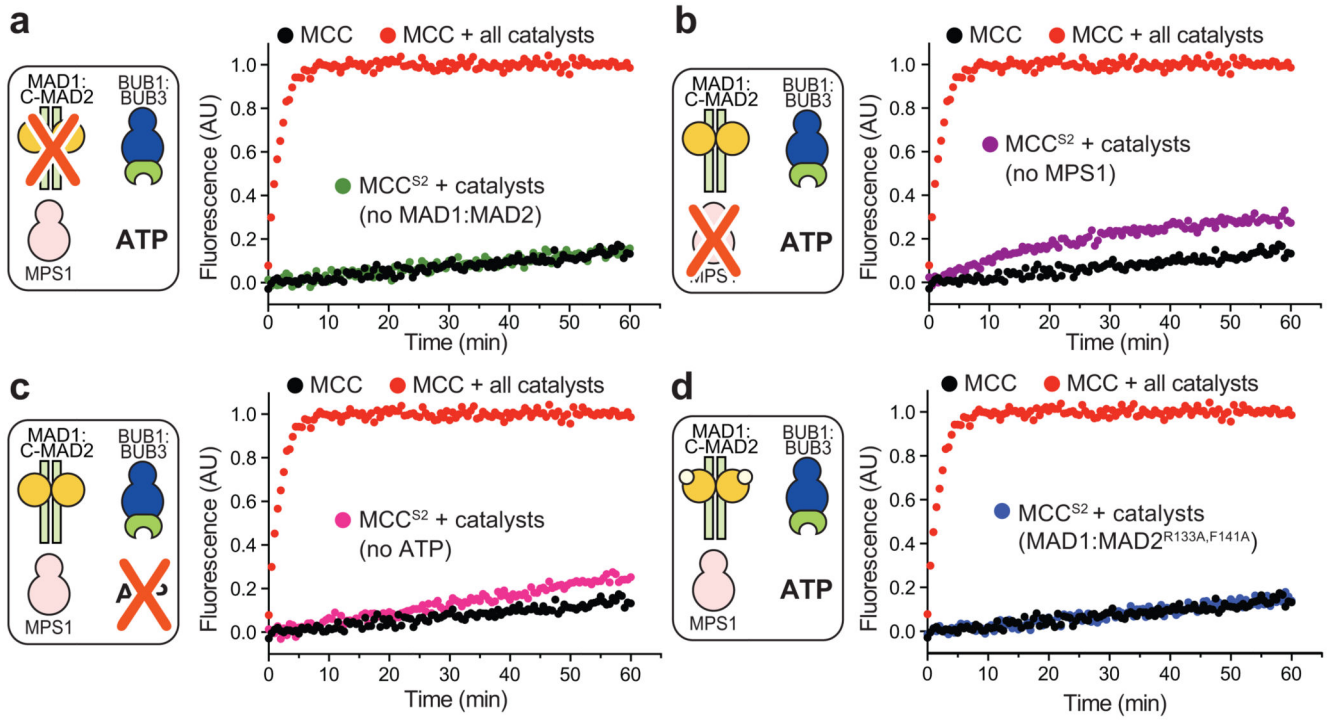

Figure 3. Molecular requirements of catalytic MCC assembly

a-c, catalytic MCC assembly requires MAD1:C-MAD2, MPS1, ATP, and BUB1:BUB3. MCC assembly was monitored with Sensor 2 as described in Figure 2b using 100 nM catalysts. Individual components were omitted as indicated. The same control profiles (black and red curves) are shown in all panels. **d**, Mutations in C-MAD2 bound to MAD1 that prevent its interaction with the sensor's O-MAD2 abrogate catalysis. Control profiles (black and red curves) are the same shown in Figure 3a-c and Extended data Figure 5a. Assay performed with sensor 2 as described in Figure 2b using 100 nM catalysts.

Europe PMC Funders Author Manuscripts

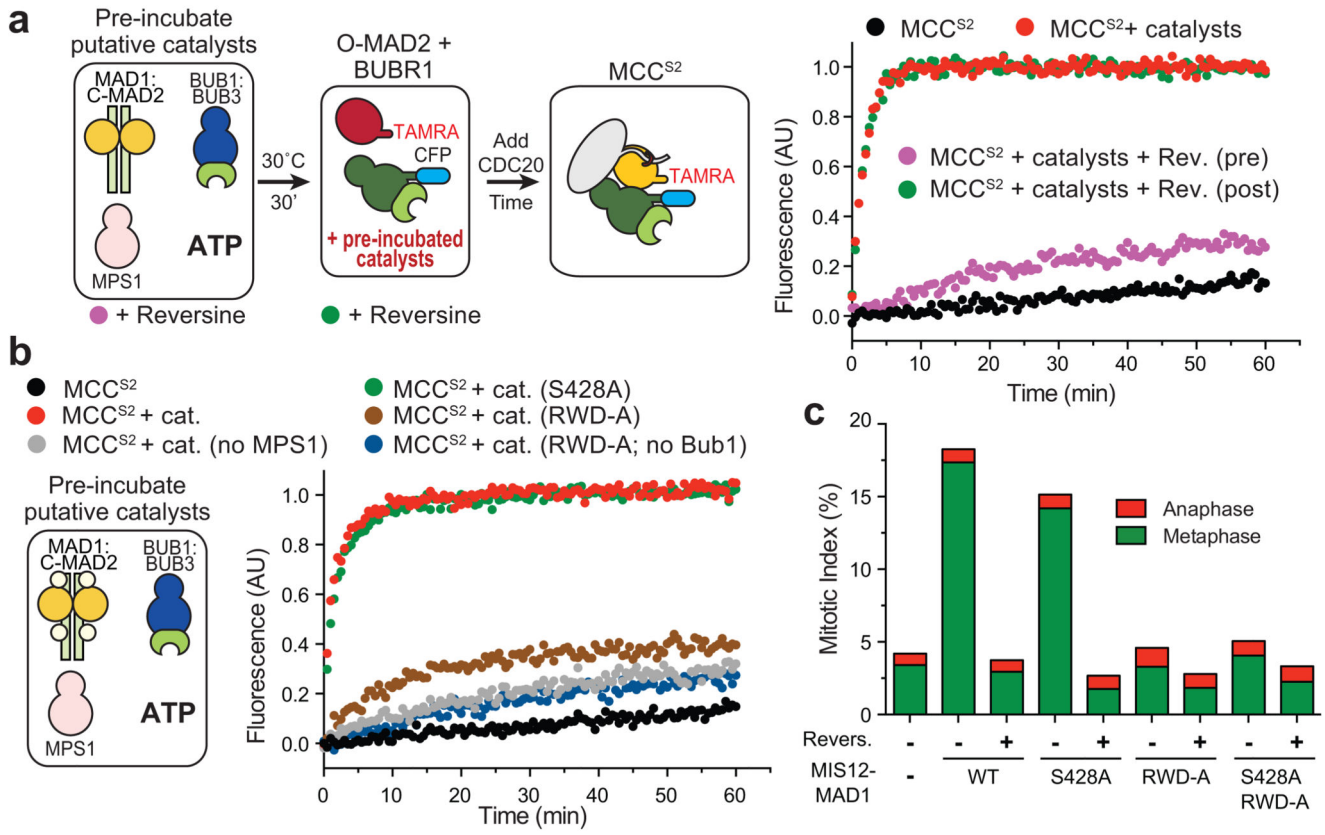

Figure 4. MPS1 activates MAD1

a, Reversine added during pre-incubation of catalysts ("pre", purple) or during MCC Sensor 2 assembly phase ("post", green). Concentration of inhibitor was 5 μM in FRET assay and 50 μM in pre-incubation. Assay performed as described in Figure 2b using 100 nM catalysts. **b**, Phosphorylation sites in the RWD domain of MAD1 ($MAD1^{RWD\text{-}A}$) are required for MCC catalysis (brown). Limited residual catalysis is due to Bub1 (compare brown and blue). Experiments conducted with $MAD1^{420\text{-}C}$ as described in Figure 2b using 100 nM catalysts. **c**, HeLa cells were transfected with mCherry (-, 1471 cells), mCherry-MIS12-MAD1WT (WT, 1451 and 1224 cells), mCherry-MIS12-$MAD1^{S428A}$ (S428A, 1309 and 1198 cells), mCherry-MIS12-$MAD1^{RWD\text{-}A}$ (RWD-A, 1838 and 1138 cells), or mCherry-MIS12-$MAD1^{S428A,RWD\text{-}A}$ (S428A-RWD-A, 1657 and 1289 cells). After 30 hours, mitotic indexes of mCherry positive cells (Extended data Figure 6b) were scored by visualization of DNA, CREST (kinetochores), and α-tubulin (not shown). Cells were also treated with 500 nM Reversine for 2 h before fixation. Graphs report mean of at least two technically independent experiments and the number of cells used for each quantification are listed above.

Europe PMC Funders Author Manuscripts

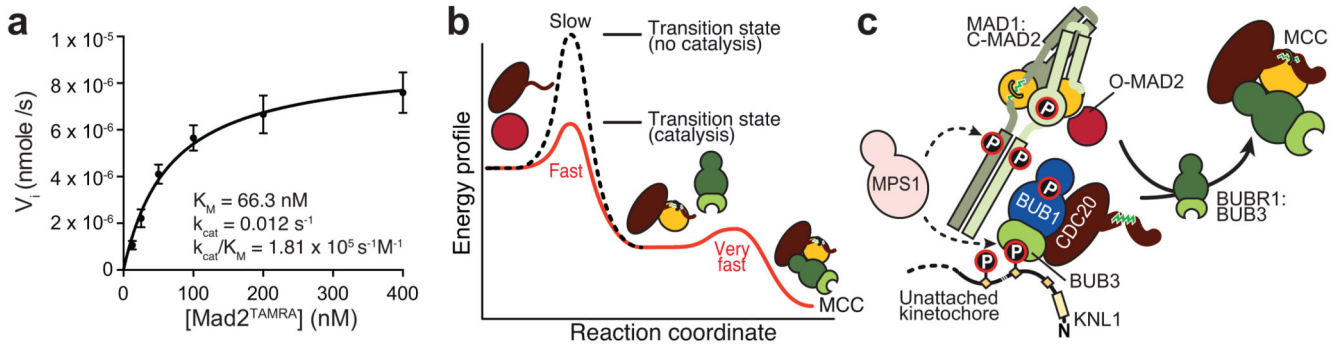

Figure 5. Role of catalysis in MAD2 activation dynamics

a, Michaelis-Menten kinetics of MCC catalysis. Catalysts were prepared as described in Figure 2b and used at 5 nM concentration; CDC20 and BUBR1 concentration was 500 nM. Bars indicate ± SEM of 3 independent technical replicates of the experiment. **b**, The catalytic apparatus of the SAC targets binding of O-MAD2 with CDC20, rate-limiting step of MCC assembly. Relative energy profiles indicate reaction is spontaneous but slow due to high activation energy. Catalysis reduces it, increasing reaction rate. Incorporation of BUBR1:BUB3 in MCC is fast and does not require catalysis. **c**, Summary drawing. MPS1 phosphorylates KNL1 to promote kinetochore recruitment of BUB1:BUB3, and MAD1:C-MAD2 to activate it and promote binding to BUB1:BUB3. MAD1:C-MAD2 and BUB1:BUB3 recruit O-MAD2 and CDC20, respectively, catalysing their interaction. Subsequent incorporation of BUBR1:BUB3 drives MCC assembly.

Europe PMC Funders Author Manuscripts